# Negative differential resistance in hybrid carbon-based structures

A. B. Felix,[1] M. Pacheco,[2] P. Orellana,[2] and A. Latgé[1]
[1]*Instituto de Física, Universidade Federal Fluminense, Niterói, Av. Litorânea sn 24210-340, Rio de Janeiro, Brazil*
[2]*Departamento de Fisica, Univ. Tec. Federico de Santa María, Casilla 110-V, Valparaíso, Chile*

(Received 15 March 2019; published 22 May 2019)

Here we study negative differential resistance effect in hybrid carbon nanostructures composed of graphene nanoribbons and carbon nanotubes. In the coupled structure, the finite flakes of nanotubes allow the formation of resonant states in the system tuning the conductance and generating Fano antiresonances. A single-band tight-binding approximation is adopted, and the density of states and conductance of the hybrid systems are calculated within the Green's function formalism and recursive numerical approaches. Armchair and zigzag edge geometries are chosen to investigate the topology effects on the electronic and transport properties for different configurations of the hybrid systems. For nanoribbons with armchair edges we derive a multiple-mode approach to analytically calculate the transmission function for the hybrid coupled system. Large and robust negative differential resistance effects are observed in the nanotube-nanoribbon zigzag hybrids that may be used in switching electronic transport responses.

DOI: 10.1103/PhysRevB.99.195442

## I. INTRODUCTION

Carbon-carbon hybrids composed mainly of graphene and other carbon allotropes have been proposed long before the achievements of recent technological advances that have allowed much progress in the area. Examples are the growth of sophisticated nanostructured materials [1–3] and the bottom-up synthesis of graphene nanoribbon [4] and nanoribbon heterojunctions [5]. Nanoporous materials composed of surface areas intercalated by tubes were designed as hydrogen storage devices and studied via first-principles calculations. The results show that when doped with lithium cations the system enhances considerably its hydrogen store capacity [6]. Additional band-edge states and energy gap modulations are two examples of how the electronic properties of graphene nanoribbons (GNRs) may be altered when they are coupling with a carbon nanotube (CNT) lying on its surface [7]. Depending on the GNR width and the CNT diameter of the hybrid systems, metal-insulator transition may be predicted and verified by scanning tunneling microscopy measurements. Spin degeneracy breaking was also numerically verified for hybrid nanotube-graphene junctions where the GNRs are directly bonded to CNTs along the sidewall [8]. Experimentally, flexible graphene nanoribbon-carbon nanotube films were fabricated by a partial unzipping process of pristine multiwalled carbon tubes [9]. In the process, residual CNTs were bonded on different GNRs as connecting bridges, forming cross-linked architectures of CNT-GNR hybrids, making easier the electron or charge transfer inside this new carbon material. Synthesis of carbon nanotube-graphene heterostructures was also addressed using microwave plasma chemical vapor deposition [10]. The graphene layers were grown on top of an aligned CNT array on a Si substrate and interconnected, forming a vertically aligned network. Alternatively, fabrication of high-speed graphene transistors with a self-aligned nanowire made of $Co_2Si$ used as a gate was reported [11]. The design allowed also high-frequency electronics performance. Also, studies of fabricated hybrid systems of multiwalled CNTs, polyvinylidene fluoride, and GNRs have provided nanocomposites with interesting dielectric properties [12].

On the other hand, CNTs on graphene nanoribbons may be viewed as a kind of defect line that is known to produce dramatic changes on the transport properties compared to idealized graphene nanoribbons [13–15]. The presence of a line defect causes a Fano effect and bound states in the continuum in the electron transport process mainly due to induced localized quantum states around the Dirac point. Nanojunctions have been theoretically described within the Landauer formalism, and the formation of localized states in the device region has been attributed to line defect formations [16]. The resulting zero conductance at the Dirac point was associated with the edge state localized at the zigzag-edged shoulder of the nanojunctions. An interesting response of the hybrid structure proposed here is the presence of negative differential resistance (NDR) observed in the characteristic curves of current versus bias voltage. NDR in graphene-based materials is a very important tool to increase their potential applications in electronic devices. Indeed, graphene superlattices are shown to reinforce the formation of NDRs at different bias voltage [17,18]

Here we address a theoretical study on such GNR-CNT hybrid systems as schematically shown in Fig. 1, i.e., a finite carbon nanotube deposited on a graphene nanoribbon, both with the same width and belonging to the same family: zigzag-zigzag [$N_Z$-ZGRN/$(n,0)$CNT] and armchair-armchair [$N_A$-AGNR/$(n,n)$CNT]. We explore possible routes of changing electronic properties of the composed systems coming from the geometries of the individual components (ribbon widths, tube radii) and from external condition fluctuations. Gases and strain, for instance, may alter the coupling energies between the different parts of the hybrid system.

We follow a single-band tight-binding approximation and real-space renormalization techniques to obtain the Green's

 

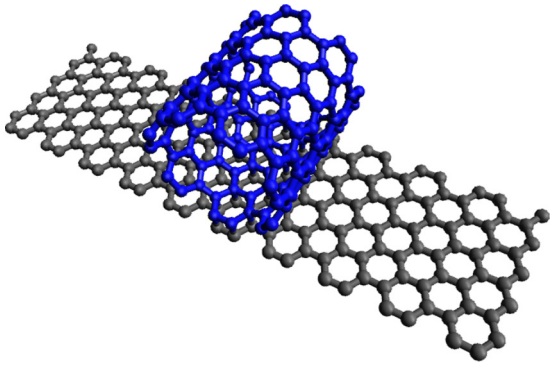

FIG. 1. Schematic view of a zigzag hybrid system: a graphene nanoribbon (10-AGNR) with a finite (7,7)CNT lying on it, both with armchair edges. The tube is perfectly superposed with the ribbon.

functions and the electronic properties of the system. The scattering formalism is used to obtain the transport transmission coefficients. Alternatively, an analytical description for the transmission coefficient is derived for the armchair case, assuming a perfect matching between the armchair GNR and the lying nanotube.

## II. TIGHT-BINDING MODEL

The system is separated into three parts: two leads and a central scattering region, and described by a $\pi$-band tight-binding Hamiltonian, written as

$$H = H_L + H_R + H_C + H_{LC} + H_{RC}, \tag{1}$$

where $H_{L(R)}$ corresponds to the left (right) lead, $H_C$ the central conductor system composed of the GNR and the CNT, and $H_{LC(RC)}$ are the connecting terms. The leads are described by pristine nanoribbons perfectly matching the central part. While the hopping energy between carbon atoms in the nanoribbon ($t$) ia considered equal to 2.75 eV [19], a smaller value is considered for the hopping between atoms at the nanoribbon and the tube in the junction ($t' = 0.2t$). For the armchair and zigzag cases, the coupling between them is given through hopping energies involving an A-B dimer pair in the strip and an A-B dimer in the tube, A and B representing the two graphene sublattices.

By following standard numerical procedures based on real-space renormalization techniques we obtain recursively the Green's functions of the system [20,21] and calculate total and local electronic density of states of a variety of such GNR-CNT hybrid systems. The conductance is obtained within the Landauer formalism [22]. Following the tight-binding approximation, it is also possible to derive analytically the transmission coefficient in the multiple-mode approximation [23] for the hybrid system composed of an armchair nanoribbon and a commensurable armchair tube on it. In the Appendix we show the analytical details to obtain the transmission, which is given by

$$T(\epsilon) = \frac{4(1-y')^2 \sin^2\theta}{(D\cos\theta - 2x')^2 + (2+D)^2 \sin^2\theta}, \tag{2}$$

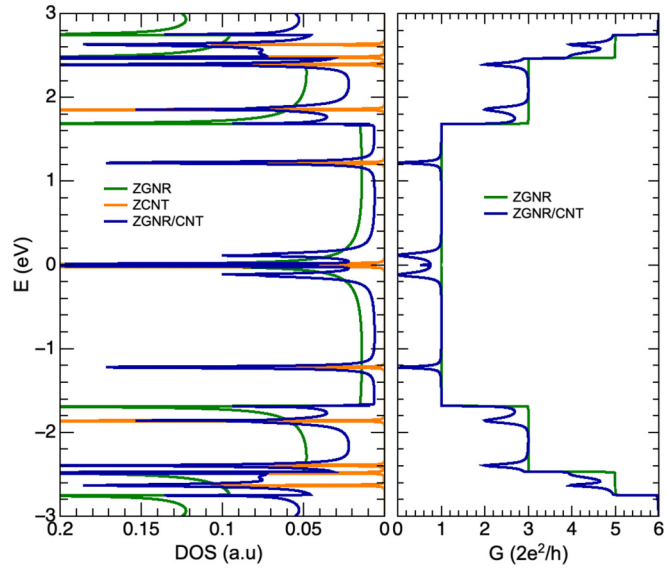


FIG. 2. DOS (left) and conductance (right) of a 6-ZGNR/(7,0)CNT (dark blue curve). The results corresponding to the DOS of the isolated ribbon and tube are shown with green and orange curves, respectively.

where $D = y'^2 - 2y' - x'$, with $x' = 2(t'/t)^2 x/z$, $y' = 2(t'/t)^2 y/z$, and

$$x = \cos kn, \;\; y = \cos(kn - \theta), \;\; z = 4\sin\theta \sin kn, \tag{3}$$

with $\theta$ being the phase difference between A and B wavefunction amplitudes.

We should remark that the information of the tube radius, defined by the number of atoms along the circumference, appears in the variables $x$, $y$, and $z$, while the lateral confinement of the ribbon defines the $q$ and $\theta$ values. The numerical results obtained for the transmission coefficients relative to armchair hybrids are in total agreement with the analytic predictions given by Eqs. (2) and (3).

## III. RESULTS

To compare the effects of each component of the hybrid system 6-ZGNR/(7,0)CNT on the electronic properties we calculate the individual density of states (DOS) of the 6-ZGNR and the (7,0) finite ZCNT. The results are shown in the left part of Fig. 2 together with the density of states of the complete hybrid system as a dark blue curve. This latter exhibits a sequence of van Hove singularities, resembling the features of the DOS of the isolated components. The corresponding conductance as a function of the Fermi energy of the system is plotted in the right panel of the same figure revealing the conductance suppression at particular energies. These correspond to the energy of the localized states of the finite tube lying on the ZGNR. Therefore, tubes of other radii reveal conductance suppressions at different energies.

Similar results for the DOS and conductance of a hybrid AGNR-CNT are shown in Fig. 3. It is interesting to notice that as a consequence of the finite size of the armchair tube, the DOS of the composed armchair system displays a pronounced peak at the Fermi energy coming from tube edge states. The

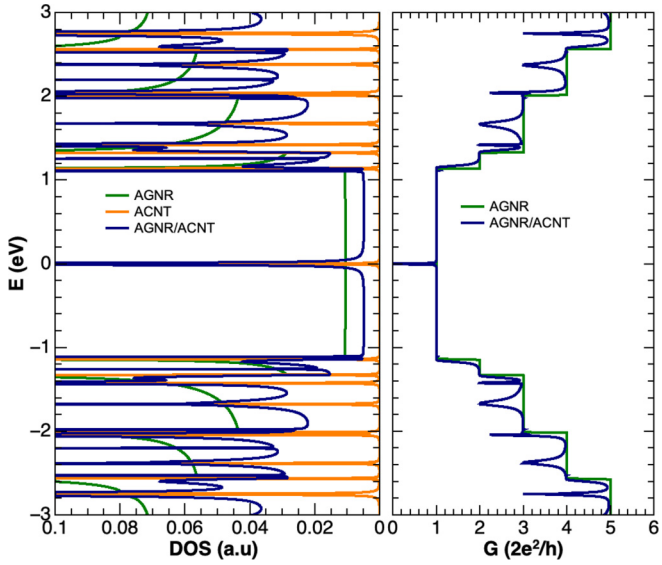


FIG. 3. DOS (left) and conductance (right) of a 11-AGNR/(7,7)CNT (dark blue curve). The results corresponding to the DOS of the isolated ribbon and tube are shown with green and orange curves, respectively.

localized nature of the new energy states of the armchair hybrid system is manifested as a suppression in the conductance at that energy. This suppression is revealed independently of the tube radius size, as shown in the conductance results displayed in Fig. 4 for hybrid systems composed of a finite $(n, n)$ tube coupled to an 8-AGNR.

Due to the coupling of the localized states of the finite nanotube and the extended states of the nanoribbon, the conductance of the hybrid systems shows a series of Fano antiresonances located at the energies corresponding to the finite tube eigenstates [24]. These are highlighted in Fig. 4 by the sequence of conductance dips in the central plateau, for armchair tubes with different diameters. The exact position

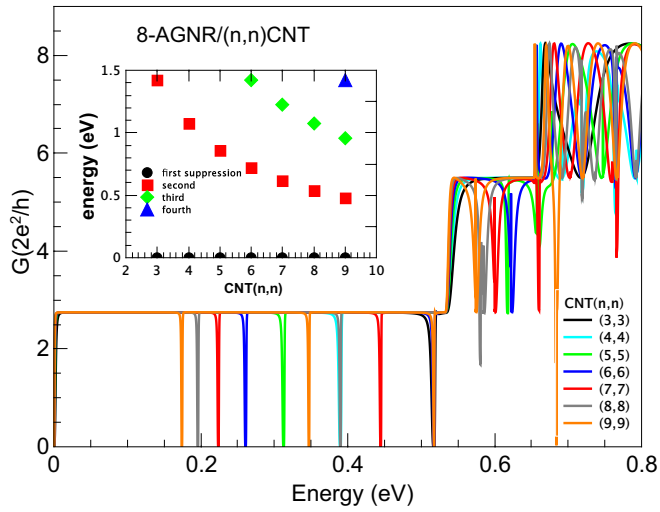


FIG. 4. Conductance results for different $(n, n)$ CNTs on an 8-AGNR. The inset shows the energy values corresponding to the conductance dips for different values of the tube index $n$.

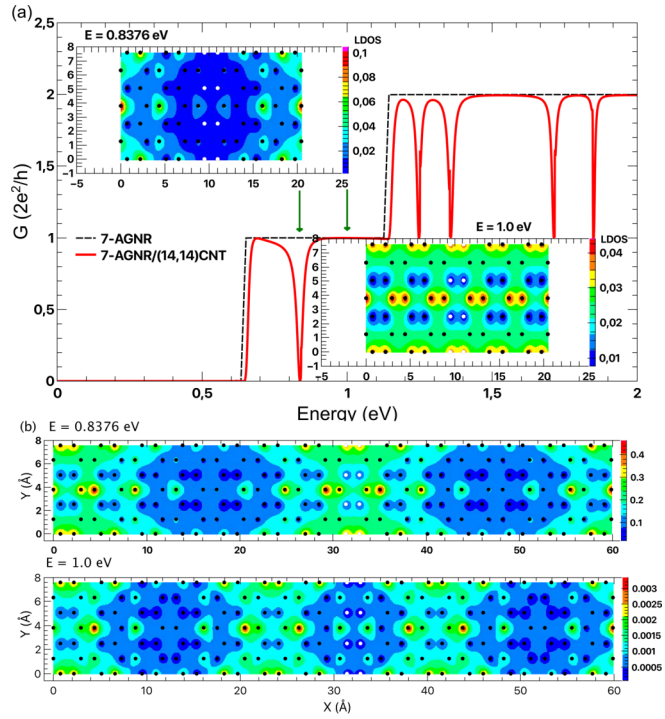


FIG. 5. (a) Conductance results of a 7-AGNR/(14,14)CNT (red curve) and the pristine 7-AGNR in a dashed line. The inset shows the nanoribbon LDOS for $E = 0.8376$ eV (left) and 1.0 eV (right). (b) LDOS results at the tube for both energies: $E = 0.8376$ eV and 1.0 eV in the top and bottom panels, respectively. The carbon sites connecting the AGNR and tube are shown with white symbols.

of the conductance antiresonances are shown in the inset as a function of the tube radius (in terms of the $n$ index). As already mentioned, all the configurations present a conductance suppression at zero energy. The second suppressions exhibit a decreasing quadratic dependence on the tube radius, given in terms of the integer $n$. All the results presented were obtained using the analytic expression [Eq. (2)] and via numerical calculation provided by recursive Green's functions.

The combination of conductance and local density of states calculations is frequently used to investigate the nature of the different electronic states. Here we present the local density of states (LDOS) of different hybrid systems. Figure 5 displays the LDOS of the 7-AGNR/(14,14)CNT hybrid system at two energy values: 0.8376 eV and 1.0 eV in a spatial contour-plot representation. The nanoribbon LDOS maps shown in Fig. 5(a) display two different features: while the transmission is total at the energy 1.0 eV, denoting a ribbon extended state and a periodic pattern for the LDOS at the ribbon (inset on the right), the electronic state corresponding to the 0.8376 eV energy (inset on the left) shows a electronic distribution localized at the contact zone with the tube, responsible for the transmission suppression. The corresponding LDOS along the tube is shown in Fig. 5(b), where the tube is shown unzipped. The connecting carbon atoms between the GNR and CNT parts are shown with white circles at the central part of the contour plots.

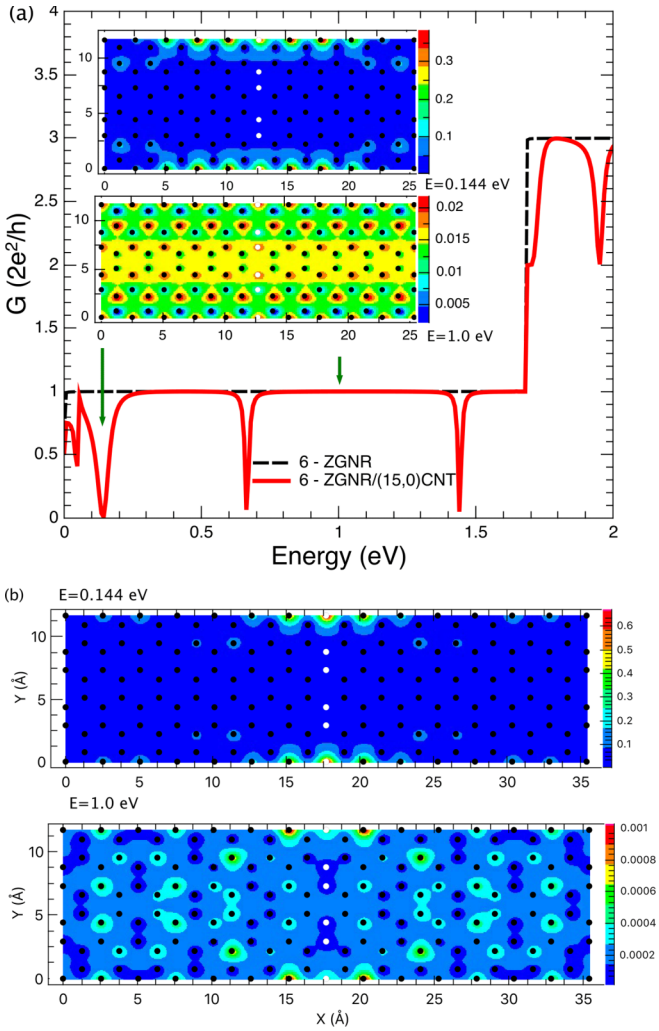


FIG. 6. (a) Conductance of a 6-ZGNR/(15,0)CNT (red curve) and the pristine 6-ZGNR (dashed line) for comparison. The inset shows the nanoribbon LDOS for $E = 0.144$ eV (top) and 1.0 eV (bottom). (b) LDOS results at the tube for both energies: $E = 0.144eV$ and 1.0 eV in the top and bottom panels, respectively. The carbon sites connecting the ZGNR and tube are represented as white symbols.

Conductance and LDOS results of a 6-ZGNR/(15,0)CNT are displayed in Fig. 6(a). The inset shows the nanoribbon LDOS for two energies, marked with green arrows. In the upper plot the high density of states at some edge carbon atoms of the ribbon, close to the nanotube flake (marked with white symbols), indicates the localized state in $E = 0.144$ eV. The second contour plot exhibits the ribbon LDOS at $E = 1.0$ eV, corresponding to a complete transmission state. The tube LDOS for the same energies is exhibited in Fig. 6(b) confirming the localized nature of the state of energy $E = 0.144$ eV.

Since the Fano antiresonances in the conductance depend on the details of the tube attached on the GNR, we investigated the current responses for a finite bias $V_{\text{Bias}}$ applied on the nanoribbon. A scattering central region is then defined by a finite number of GNR unit cells (defined here as $d$) including the tube on top of it, coupled at left and right

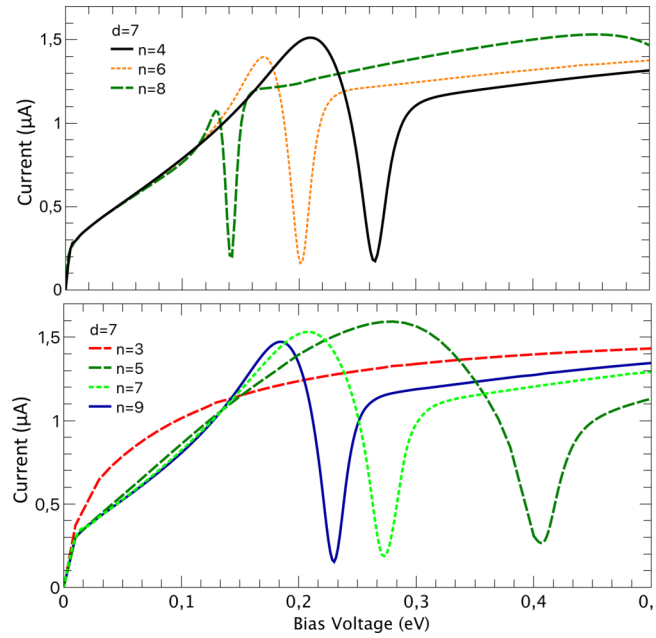


FIG. 7. Current versus bias voltage for 6-ZGNR/($n$,0)CNTs considering distinct $n$ values and $d = 7$. Top and bottom panels are for even-$n$ and odd-$n$ values, respectively, and $T = 1$ K.

to perfect nanoribbon leads that are at different chemical potential ($\mu_{L,R}$). A linear potential drop within the scattering region is considered. For the sake of simplicity the tube is considered at null potential energy. The current was calculated within the Landauer-Buttiker formalism,

$$I(V_{\text{Bias}}) = \frac{2e}{h}\int d\epsilon[f(\epsilon-\mu_L) - f(\epsilon-\mu_R)]T(\epsilon, V_{\text{Bias}}), \tag{4}$$

with the chemical potential given by $\mu_{L,R} = \pm V_{\text{Bias}}/2$.

In Fig. 7 we present the results of the current versus voltage for the hybrid system 6-ZGNR/($n$,0)CNT considering a fixed scattering region $d = 7$, and different values for the index $n$. To analyze the current dependence on the tube size, we displayed the cases of even $n$ (4, 6, 8) and odd $n$ (3, 5, 7, 9) in two panels (top and bottom, respectively). Different behavior of the I-V characteristic is expected for $n$-even and $n$-odd parity due to the particular symmetries of the carbon atom distributions along the nanotube with respect to the nanoribbon. Here we take the connecting position line between the tube and the ribbon as the reference axis.

For both cases a dip in the current is evident, and it takes place at decreasing bias voltage values as the tube radius increases. Actually, the energy value at which the current depression occurs is correlated with the antiresonances observed in the transmission results. More explicitly, these particular energy values for the current dips are found to be almost twice the corresponding antiresonances in the conductance for all the tube radii considered. This can be understood as being the bias necessary to achieve the resonant condition, i.e., $\epsilon_r = V_0/2$.

We notice that a large NDR effect appears for all the 6-ZGNR/($n$,0) CNTs studied, indicating that these hybrid systems can be used to improve transport responses in a

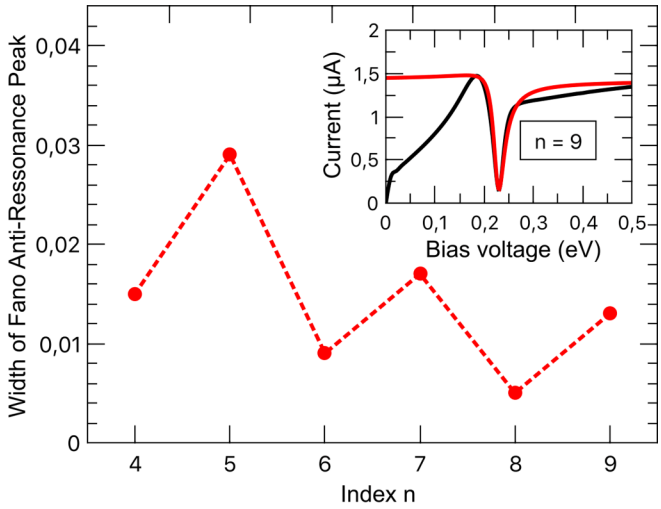


FIG. 8. Dependence of the width of the Fano antiresonance on the tube radius (given in the integer $n$). Inset: Fano fitting of the current dip observed for the current versus bias voltage for a 6-ZGNR/(9,0)CNT, $d = 7$, and $T = 1$ K.

controllable way. As in the case of the linear conductance, the current dips are Fano antiresonances. We have fitted all the current results shown in Fig. 7 for the even and odd tubes into the Fano equation, described analytically by

$$F(V_{\text{Bias}}) = \gamma \frac{((V_{\text{Bias}} - V_o)/\Gamma + q_r)^2 + q_i^2}{\left(1 + q_i^2 + q_r^2\right)(1 + (V_{\text{Bias}} - V_0)^2/\Gamma^2)} \qquad (5)$$

with $\gamma$ being a constant of proportionality, and $\Gamma$ the line width of the Fano curve, and where $V_0$ is the energy value at which the Fano resonance takes place, and $q_r$ and $q_i$ are the real and imaginary parts, respectively of the Fano parameter $q$ which measures the ratio of resonant scattering to the direct scattering amplitude. The dependence of the width of the Fano antiresonance on the tube radius is depicted in Fig. 8. In the inset we show the current dip observed in the current versus bias voltage for a 6-ZGNR/(9,0)CNT and $d = 7$ together with a fitted curve (red line) using the Fano function given in Eq. (5). The fitting is excellent, endorsing the idea that the characteristic curves provide evidence of the interference Fano effect occurring in the hybrid systems.

When a finite bias is applied, the current through the system depends on the size of the scattering region between the leads. We have investigated this effect for a hybrid 6-ZGNR/(4,0)CNT with $d = 3, 5$, and 7, and the results are shown in Fig. 9(a). We noticed that the peak-valley ratio is essentially determined by the size of the scattering region. For comparison, the current versus bias for isolated pristine nanoribbons, for the same scattering region sizes are displayed in dashed lines. As expected, no peak-valley features are exhibited. The temperature dependence of the I-V characteristic curves is presented in Fig. 9(b) for the same hybrid system and $d = 5$. Although the peak-to-valley ratio decreases as the temperature increases the position at which the current dip happens is robust against temperature changes. The presence of other tubes on the nanoribbons was also explored. The results reveal that the ranges of the voltage values at which NDRs occur depend on the distance between the tubes besides

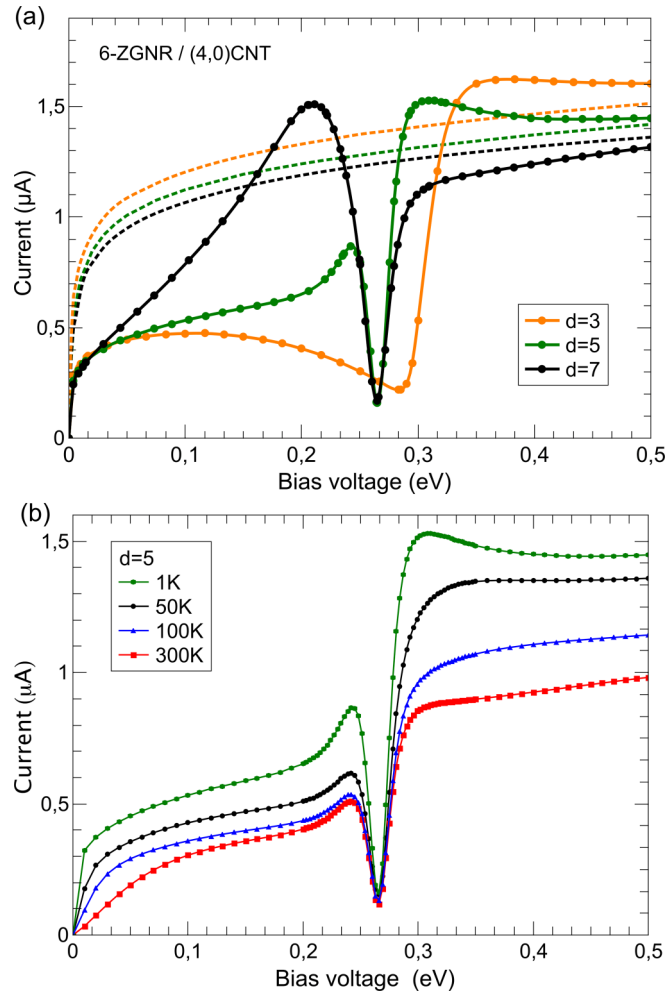


FIG. 9. Current versus bias voltage for an 6-ZGNR with (a) a (4,0)CNT on it for three distinct sizes of the scattering region with the potential drop ($d = 3$, 5, and 7), and $T = 1$ K.

symmetry aspects of the hybrid configuration that should be prepared within sophisticated synthesis processes [4,5].

The analysis of the current was extended to armchair hybrid systems (armchair tubes on armchair nanoribbons). The results for semiconducting GNRs (families $3p$ and $3p + 1$) are shown in Fig. 10, considering different scattering regions ($d = 3$, 5, and 7) and small tube radii ($n = 3$ and 5). Differently from the zigzag counterpart the armchair hybrids do not exhibit NDR features, and the current characteristic curves are similar to the observed for isolated GNRs. A standard ohmic-like behavior was achieved for the metallic $3p + 2$ armchair family, shown in the inset of the figure, due essentially to the existence of a large plateau of complete transmission for low energies. A light deviation from the ideal transport situation (dashed lines in the inset) was found, however, since a small gap is opened at zero energy, as shown previously in Fig. 3 for tubes with different radii and scattering region sizes ($n$ and $d$ parameters, respectively).

## IV. FINAL REMARKS

We have presented a theoretical study of the effects of CNTs coupled to graphene nanoribbons on the transport

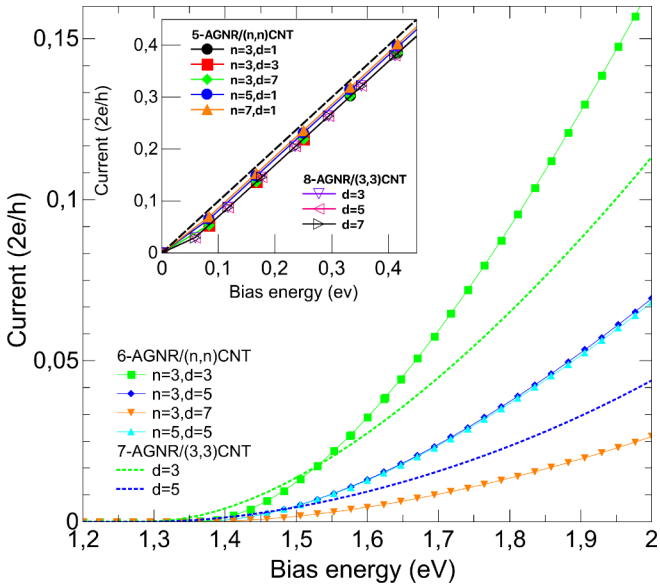


FIG. 10. Current versus bias voltage for $m$-AGNR/$(n, n)$ACNT, with $m = 6$ and $m = 7$, with different central scattering conductors ($d = 3$, 5, and 7), distinct armchair tubes ($n = 3$ and 5) and $T = 1$ K. Inset: Metallic family with $m = 5$ and 8, and $d = 1$, 3, 5, and 7.

responses. A tight-binding approximation was used following real-space renormalization schemes within the Green's function formalism. For GNRs with armchair edges we derive a multiple-mode approach to analytically calculate the transmission function for the hybrid system. We have explored the possibility of generating Fano antiresonances and tuning conductance by varying the topology of the hybrid systems. The zigzag arrangement has proven to exhibit interesting and robust negative differential resistance at a given range of voltage values that may be controlled. Considering the results the hybrid systems can be used as new routes for interesting possibilities of switching electronic transport responses, very similarly to the case of defect lines in graphene nanoribbons.

## ACKNOWLEDGMENTS

The work has been partially financially by Brazilian agencies CAPES, CNPq, and FAPERJ and the Chilean Government through the FONDECYT Grant No. 1151316. P.O. thanks UTFSM DGIIP for an internal grant. A.L. would like to acknowledge the financial support of FAPERJ under Grants No. E-26/101.522/2013 and No. E-26/202.953/2016 and the INCT de Nanomateriais de Carbono.

## APPENDIX: ANALYTICAL CALCULATION

Starting from an isolated armchair graphene nanoribbon we write the equation of motion for the probability amplitudes of finding an electron at the $jm$ site of the atomic $A$ and $B$ sublattices,

$$\epsilon\Psi^A_{jm} = t\Psi^B_{jm} + t\Psi^B_{j-1,m+1} + t\Psi^B_{j-1,m-1},$$
$$\epsilon\Psi^B_{jm} = t\Psi^A_{jm} + t\Psi^A_{j+1,m-1} + t\Psi^A_{j+1,m+1}, \quad \text{(A1)}$$

with $t$ being the hopping energy between the first neighboring atoms in the ribbon. The electronic wave function may be written as $\Psi^{A(B)}_{j,m} = \Phi^{A(B)}_j e^{iqm}$, with $q$ being defined by the lateral ribbon confinement [25], and we get

$$\epsilon\Phi^{A(B)}_j = t\Phi^{B(A)}_j + 2t\Phi^{B(A)}_{j-1(j+1)}\cos q. \quad \text{(A2)}$$

Now, taking into account the translation symmetry along the isolated ribbon we write $\Phi^{A(B)}_j = A(B)e^{ik_j}$, which leads to the well-known energy relation $\epsilon(q, k) = t\sqrt{1 + 4\cos^2 q + 4\cos q\,\cos k}$. Also, we get that the amplitudes $A$ and $B$ are related by

$$B = \left(\frac{1 + 2\cos q\, e^{ik}}{\epsilon}\right)A = e^{i\theta}A, \quad \text{(A3)}$$

where the phase depends on the energy, $\theta = \theta(k, q)$.

When a finite carbon nanotube, of the same extension and chirality of the armchair GNR, is considered lying on the ribbon, an extra term appears:

$$\epsilon\Phi^{A(B)}_j = t\Phi^{B(A)}_j + t'\alpha_1(\beta_1)\delta_{j,0} + 2t\Phi^{B(A)}_{j-1(j+1)}\cos q, \quad \text{(A4)}$$

where $\alpha_1$ and $\beta_1$ refer to the electronic wave functions of the CNT trapped on the nanoribbon and $t'$ is the hopping energy between first-neighbor carbon atoms, one at the tube and the other at the zero position of the ribbon. Equivalent equations are written for the tube:

$$\epsilon\alpha_l = t\beta_l + 2t\cos q\,\beta_{l-1} + t'\Phi^A_0\delta_{l,0},$$
$$\epsilon\beta_l = t\alpha_l + 2t\cos q\,\alpha_{l+1} + t'\Phi^B_0\delta_{l,0}. \quad \text{(A5)}$$

Considering a finite armchair tube $(m, m)$, the number of dimers along the tube circumference is given by $M = 2m$. This means that applying the tube boundary conditions in Eq. (5), for $l = 1$ and $l = M$, we have

$$\epsilon\alpha_1 = t\beta_1 + 2t\cos q\,\beta_M + t'\Phi^A_0,$$
$$\epsilon\beta_1 = t\alpha_1 + 2t\cos q\,\alpha_2 + t'\Phi^B_0,$$
$$\epsilon\alpha_M = t\beta_M + 2t\cos q\,\beta_{M-1},$$
$$\epsilon\beta_M = t\alpha_M + 2t\cos q\,\alpha_1. \quad \text{(A6)}$$

To obtain the transmission probability we consider incoming, reflected, and transmitted wave function components along the longitudinal direction and take into account the phase difference $\theta$ between $A$ and $B$ amplitudes.

[1] C. Tan, J. Chen, X.-J. Wu, and H. Zhang, Nat. Rev. Mater. **3**, 17089 (2018).
[2] J. D. Correa, P. A. Orellana, and M. Pacheco, Nanomaterials **7**, 69 (2017).
[3] O. V. Kharissova, B. I. Kharisov, and C. M. O. Gonzalez, Ind. Eng. Chem. Res. **58**, 3921 (2019).
[4] J. Cai, P. Ruffieux, R. Jaafar, M. Bieri, T. Braun, S. Blankenburg, M. Muoth, A. P. Seitsonen, M. Saleh, X.

Feng, K. Mullen, and R. Fasel, Nature (London) **466**, 470 (2010).
[5] C. Bronner, R. A. Durr, D. J. Rizzo, Y.-L. Lee, T. Marangoni, A. M. Kalayjian, H. Rodriguez, W. Zhao, S. G. Louie, F. R. Fischer, and M. F. Crommie, ACS Nano **12**, 2193 (2018).
[6] G. Dimitrakakis, E. Tylianakis, and G. Froudakis, Nano Lett. **8**, 3166 (2008).
[7] T. S. Li, S. C. Chang, and M. F. Lin, Nanotechnology **19**, 105703 (2008).
[8] Z. Qu, L. Gu, M. Li, G. Shi, and G.-L. Zhuang, Phys. Chem. Chem. Phys. **15**, 20281 (2013).
[9] M. Liu, Y. Du, Y.-E. Miao, Q. Ding, S. He, W. W. Tjiu, J. Pan, and T. Liu, Nanoscale **7**, 1037 (2015).
[10] C. S. Rout, A. Kumar, T. S. Fisher, U. K. Gautam, Y. Bandoc, and D. Golberg, RSC Adv. **2**, 8250 (2012).
[11] L. Liao, Y.-C. Lin, M. Bao, R. Cheng, J. Bai, Y. Liu, Y. Qu, K. L. Wang, Y. Huang, and X. Duan, Nature (London) **467**, 305 (2010).
[12] M. Arjmand, S. Sadeghi, M. Khajehpour, and U. Sundararaj, J. Phys. Chem. C **121**, 169 (2017).
[13] W.-J. Gong, X.-Y. Sui, Y. Wang, G.-D. Yu, and X.-H. Chen, Nano. Res. Lett. **8**, 330 (2013).
[14] X. Lin and J. Ni, Phys. Rev. B **84**, 075461 (2011).
[15] Y. Han, X.-Y. Sui, and W.-J. Gong, J. Appl. Phys. **113**, 233701 (2013).
[16] H. Li, R. Li, Q. Yu, X. Kang, and J. Ding, Solid State Commun. **233**, 18 (2016).
[17] G. J. Ferreira, M. N. Leuenberger, D. Loss, and J. C. Egues, Phys. Rev. B **84**, 125453 (2011).
[18] P. Tseng, C. H. Chen, S. A. Hsu, and W. J. Hsueh, Phys. Lett. A **382**, 1427 (2018).
[19] A. H. Castro Neto, F. Guinea, N. M. R. Peres, K. S. Novoselov, and A. K. Geim, Rev. Mod. Phys. **81**, 109 (2009).
[20] C. Ritter, S. S. Makler, and A. Latgé, Phys. Rev. B **77**, 195443 (2008).
[21] V. Torres, C. León, D. Faria, and A. Latgé, Phys. Rev. B **95**, 045425 (2017); V. Torres, D. Faria, and A. Latgé, *ibid.* **97**, 165429 (2018).
[22] S. Datta, *Electronic Transport in Mesoscopic Systems* (Cambridge University Press, New York, 1995).
[23] P. A. Orellana, L. Rosales, L. Chico, and M. Pacheco, J. Appl. Phys. **113**, 213710 (2013).
[24] L. Rosales, M. Pacheco, Z. Barticevic, A. Latgé, and P. A. Orellana, Nanotechnology **19**, 065402 (2008); **20**, 095705 (2009).
[25] K. Wakabayashi, K.-I. Sasaki, T. Nakanishi, and T. Enoki, Sci. Tech. Adv. Mat. **11**, 054504 (2010).